Protofibrillar Islet Amyloid Polypeptide Permeabilizes Synthetic Vesicles by a Pore-like Mechanism that May Be Relevant to Type II Diabetes[†]

Magdalena Anguiano, Richard J. Nowak, and Peter T. Lansbury, Jr.*

Center for Neurologic Diseases, Brigham and Women's Hospital, and Department of Neurology, Harvard Medical School, 65 Landsdowne Street, Cambridge, Massachusetts 02139

Received April 26, 2002; Revised Manuscript Received June 24, 2002

ABSTRACT: Islet amyloid polypeptide (IAPP) and insulin are copackaged and cosecreted by pancreatic islet β-cells. Non-insulin-dependent (type II) diabetes mellitus (NIDDM) is characterized by dysfunction and depletion of these β-cells and also, in more than 90% of patients, amyloid plaques containing fibrillar IAPP. An aggregated but not necessarily fibrillar form of IAPP is toxic in cell culture, suggesting that prefibrillar oligomeric (protofibrillar) IAPP may be pathogenic. We report here that IAPP generates oligomeric species in vitro that are consumed as β-sheet-rich fibrils grow. Protofibrillar IAPP, like protofibrillar α-synuclein, which is implicated in Parkinson's disease pathogenesis, permeabilizes synthetic vesicles by a pore-like mechanism. The formation of the IAPP amyloid pore is temporally correlated to the formation of early IAPP oligomers and its disappearance to the appearance of amyloid fibrils. Neither pores nor oligomers were formed by the nonfibrillogenic rat IAPP variant. The IAPP amyloid pore may be critical to the pathogenic mechanism of NIDDM, as other amyloid pores may be to Alzheimer's disease and Parkinson's disease.

Ordered protein aggregation associated with fibril formation may be the molecular basis of a number of age-associated neurodegenerative diseases, including Alzheimer's disease (AD),[1] Huntington's disease, (HD), and Parkinson's disease (PD), as well as systemic diseases such as cataract formation (*1*, *2*). Non-insulin-dependent (type II) diabetes mellitus (NIDDM) has been proposed to be a member of this group, based on the fact that more than 90% of patients have extracellular amyloid deposits localized to the dysfunctional and degenerating portion of the pancreatic islets (*3*−*5*). NIDDM is a prevalent age-associated disease characterized by continuous hyperglycemia, peripheral insulin resistance, and impaired insulin secretion as well as pancreatic islet amyloid formation (*3*, *6*). Pancreatic islet amyloid fibrils comprise mainly islet amyloid polypeptide (IAPP) (*7*), a 37-amino acid peptide hormone (Figure 1) (*8*, *9*) that is normally cosecreted with insulin by islet β-cells (*10*−*12*). Since secretion of these two peptides is coregulated, it has been proposed that IAPP may modulate the effects of insulin on glucose metabolism (*13*) and stimulate lipolysis (*14*, *15*).

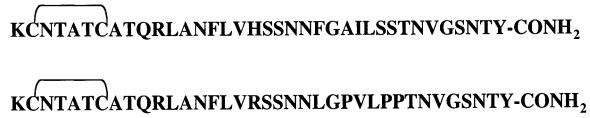

FIGURE 1: Sequence alignment for human IAPP (top) and rIAPP (bottom). These peptides differ in the central region comprising amino acids 20−29. This region is critical for fibril formation (*16*, *17*). The Cys−Cys disulfide bond is shown.

Although it is not clear whether insulin resistance, β-cell dysfunction, IAPP amyloid formation, or a combination of these is the pathogenic trigger of NIDDM, fibril formation seems to be a critical pathogenic event (*3*, *4*, *9*). First, in vitro biophysical studies of IAPP link its pathogenicity to its ability to fibrillize; nonfibrillogenic IAPP variants from cat and rat do not fibrillize, and these animals are not susceptible to NIDDM (*16*−*18*). Second, a missense mutation in IAPP (S20G) that is linked to NIDDM (*19*) promotes the in vitro fibrillization of IAPP (*20*, *21*). Third, an aggregated form of IAPP is toxic to cultured human pancreatic β-cells (*22*). Fourth, overexpression of IAPP in COS cells leads to intracellular IAPP aggregates and cell death (*23*, *24*). Finally, transgenic mice expressing IAPP produce intracellular IAPP aggregates and subsequently develop hyperglycemia (*3*, *4*, *9*, *25*−*28*).

The correlation of IAPP fibrillization and NIDDM does not require that the end-product amyloid fibril be the pathogenic species. In fact, biophysical studies of the amyloidogenic proteins associated with other diseases, primarily AD and PD, suggest that the fibril itself may be inert (*29*, *30*). In vitro amyloid fibril formation proceeds via transient, β-sheet-rich oligomers that eventually go on to form more stable fibrils (*31*, *32*). These intermediates, termed protofibrils, were first identified in the case of Aβ (*31*, *33*,

[†] This work was funded by the National Institutes of Health (Grant AG 08470).

* To whom all correspondence should be addressed. Telephone: (617) 768-8610. Fax: (617) 768-8606. E-mail: plansbury@rics.bwh.harvard.edu.

[1] Abbreviations: Aβ, amyloid-β protein; AD, Alzheimer's disease; AFM, atomic force microscopy; CD, circular dichroism; CR, congo red; EM, electron microscopy; FITC-dextran, fluorescein isothiocyanate conjugated to dextran; HBS, HEPES-buffered saline; HD, Huntington's disease; HFIP, 1,1,1,3,3,3-hexafluoro-2-propanol; HPLC, high-pressure liquid chromatography; HT-LS, high-throughput light scattering; IAPP, human islet amyloid polypeptide; rIAPP, rat islet amyloid polypeptide; MW, molecular weight; NIDDM, non-insulin-dependent diabetes mellitus; PD, Parkinson's disease; PG, phosphatidylglycerol; Thio T, thioflavin T; LS, light scattering; UV, ultraviolet−visible light spectroscopy; RT, room temperature.

10.1021/bi020314u CCC: $22.00
Published on Web 08/24/2002

34) and subsequently for α-synuclein (*35*) and transthyretin (*36*). IAPP fibrillization also proceeds via a protofibrillar intermediate (*18*, *37*), which can be detected by fluorescence anisotropy and light scattering (*38*, *39*). In the cases of Aβ and α-synuclein, in vitro analogues of potentially pathogenic properties are associated specifically with the protofibrillar species; Aβ protofibrils, for example, induce toxicity in cultured primary cortical neurons (*40*), and α-synuclein protofibrils, but not fibrils, permeabilize synthetic vesicles (*41*, *42*).

In vitro IAPP toxicity correlates with its conversion to β-sheet-containing aggregates (*27*, *38*, *43*). Although the biological targets of the putatively toxic IAPP aggregates are not known, several in vitro studies have implicated cell membranes. Membrane disruption was shown to be a property of "intermediate-sized" IAPP oligomers, but not mature IAPP fibrils (*44*). Channel-like properties of IAPP (but not rIAPP) have been described (*45*, *46*), and have recently been linked to the ability of IAPP to oligomerize (*47*, *48*).

We report here that protofibrillar IAPP permeabilizes synthetic phospholipid vesicles in a pore-like manner, allowing transit of calcium, but not larger molecules. The permeabilizing species, or "amyloid pore", is formed slowly and disappears as fibrils appear, consistent with it being one of the oligomeric species that constitute heterogeneous protofibrillar IAPP. This finding raises the possibility that NIDDM, like PD, AD, and other neurodegenerative diseases, may be initiated by protofibrillar amyloid pores.

EXPERIMENTAL PROCEDURES

Preparation of IAPP for Aggregation Assays. All the reagents were obtained from Sigma-Aldrich (St. Louis, MO) unless otherwise stated. Human IAPP (IAPP) or rat IAPP (rIAPP) (Bachem, Torrance, CA) was dissolved in HFIP (0.5 mg/mL) and sonicated for 2 min. The solution was freeze-dried overnight. The lyophilized product was then dissolved in water (0.36 mg/mL) and spun for 10 min at 20000*g*. Aggregation experiments were initiated by diluting the peptide stock solution into buffer and quickly filtering the mixture through a 0.2 μm filter (Millipore, Bedford, MA). Final peptide concentrations were 28−34 μM (based on amino acid analysis), and the buffer composition was 10 mM Tris-HCl (pH 7). Samples were incubated at either RT or 37 °C along with buffer blanks.

Thioflavin T Assay of Amyloid Fibril Formation. Fibrillization of peptide samples was monitored by a thioflavin T (Thio T) dye binding assay. Aliquots (10 μL) collected intermittently during aggregation were mixed with a Thio T stock solution [2.5 μM in 0.1 M glycine-NaOH (pH 8.5)] and incubated for 3 min at RT. Final concentrations in the measurement solution were 6−7 μM IAPP and 2 μM Thio T. Fluorescence measurements were carried out using an Analyst microplate analyzer from LJL Biosystems (excitation at 440 nm, bandwidth of 20 nm; emission at 500 nm, bandwidth of 30 nm). All measurements were carried out in duplicate and corrected for background fluorescence.

Circular Dichroism Spectroscopy for Following Secondary Structure Formation. For CD studies without vesicles, an IAPP sample (300 μL, 28 μM) was prepared as described above. For CD studies with vesicles, an IAPP sample (300 μL, 7 μM final concentration) was prepared in Tris-buffered saline and diluted by half with buffer containing 20 mM $CaCl_2$. To this mixture was added an equal volume of previously diluted vesicles (in Tris; see the vesicle permeability measurements below). Samples with or without vesicles were placed in a 0.1 cm quartz cuvette and monitored at RT from 195 to 250 nm using an Aviv 62 A DS spectropolarimeter. Spectral data were collected at 1 nm intervals with a time constant of 4 s per measurement and a bandwidth of 1 nm. The final spectrum represents an average of three individual scans after baseline (buffer alone) subtraction for samples without vesicles, and a single scan after baseline (buffer plus vesicles) subtraction for samples with vesicles.

Preparation of Phospholipid Vesicles for the Permeabilization Assay. Synthetic vesicles were prepared as previously reported by our laboratory (*41*). Briefly, PG (Avanti Polar Lipids Inc., Alabaster, AL) was dissolved in a chloroform/methanol mixture (2:1, v/v) at a concentration of 20 mg/mL. The solvent was removed by rotary evaporation, yielding a lipid film. The lipid film was thoroughly dried overnight in a lyophilizer to remove residual organic solvent. The residual lipid was hydrated with 1 mL of HBS [10 mM HEPES and 140 mM KCl (pH 7.4)] containing 1 mM EDTA, 100 mg of 1 mm diameter glass beads, and either Fura-2 (100 μM, MW = 832, Molecular Probes) or FITC-dextran 4000 (62 μM, MW = 4400). For CD studies, the lipid was hydrated with 1 mL of Tris-buffered saline [10 mM Tris and 140 mM KCl (pH 7.4)] without any probes. The mixture was spun for 30 min in a rotary evaporation system without vacuum. The vesicle suspension was then allowed to stand at RT for 2 h before downsizing. Downsizing was done by extrusion by forcing the vesicle suspension, at least 11 times, through a nuclepore polycarbonate track-etch membrane (pore size of 100 nm, Whatman). Nonencapsulated probes were removed from vesicles into HBS containing 1 mM EDTA using either a PD-10 column (Amersham Pharmacia Biotech, Uppsala, Sweden) for Fura-2 or a Superose 12 size-exclusion column (HR 10/30, 0.5 mL/min) for FITC-dextran. Purified vesicles were protected from light and stored at 4 °C for up to a few days.

Assessment of Vesicle Permeabilization to Calcium. Aliquots from aggregation experiments were diluted by half with HBS containing 20 mM $CaCl_2$ and mixed with an equal volume of vesicles previously diluted 10-fold with HBS. The sample was incubated for 15 min at RT in the dark. Following the incubation, 5 μL of the mixture was injected through an HPLC Kratos fluorescence detector (F4T5BL lamp; excitation filter, 334 nm with a 10 nm band-pass; emission filter, long-pass with a 495 nm cutoff) using a syringe pump (PHD 2000, Harvard Apparatus) with a 9725i Rheodyne injector (*41*). The running buffer was HBS and 5 mM $CaCl_2$, and the flow rate was 0.5 mL/min. For each experiment, a negative control (HBS, 5 mM $CaCl_2$, and vesicles) and a positive control (31 nM ionomycin) were run. Data from the detector were digitized at 10 Hz (Waters SAT/IN module), and the total signal was determined by integration of the peak area in the chromatogram using Waters Millenium[32] software (Waters, Milford, MA). The effect was reported as a percentage of the ionomycin effect (100%) and represents the average of three measurements.

Assessment of Vesicle Permeabilization to Larger Molecules. Aliquots from aggregation experiments were diluted by half with HBS and 20 mM $CaCl_2$ and mixed with an equal volume of vesicles previously diluted 10-fold with HBS. Following incubation for 15 min at RT, the vesicle/peptide mixture was ultrafiltered (Microcon 100, 13000*g* for 6 min). The filters were prewashed with 60 μL of HBS (13000*g* for 6 min) to reduce background absorbance and fluorescence. Triton X-100 (0.5% final concentration) was used as a positive control. Triton X-100 blank showed no interference with the relevant spectral properties. The filtrate was collected and injected using a Waters Alliance 2690 HPLC system. A constant flow rate of 0.5 mL/min was maintained with buffer (HBS and 5 mM $CaCl_2$). The extent of leakage of each molecule was determined by the following detectors in line: Kratos fluorescence detector (Fura-2, details above), Waters 474 fluorescence detector (FITC-dextran; excitation at 490 nm, 18 nm bandwidth; emission at 520 nm, 10 nm bandwidth). The total signal was determined by integration of the peak area in the chromatogram using Waters Millenium[32] software.

Electron Microscopy of IAPP Fibrils. Aliquots (5 μL) collected at different times during aggregation were adsorbed onto glow-discharged carbon-coated copper grids (2 min). Excess sample was adsorbed onto a filter paper. Grids were washed with water (5 μL) and then stained with freshly prepared 0.75% uranyl acetate (5 μL, 2 min). Samples were examined in a JEOL 1200 EX transmission electron microscope at 60 kV.

Assessment of Soluble IAPP Oligomers by Light Scattering. Total soluble protein was analyzed by a high-throughput static light scattering method (HT-LS). Aliquots of sample incubations were centrifuged (14000*g* for 2−5 min) to remove fibrillar IAPP. The supernatant (soluble protein fraction) was injected through an in-line ultrafiltration device using an Agilent 1100 series HPLC autoinjector. A constant flow rate with incubation buffer (Tris) of 0.5 mL/min was maintained by an Agilent 1100 series isocratic pump. Scattered light (90°) and UV absorbance (220 nm) were monitored by a DAWN EOS multiangle light scattering detector (Wyatt Technology, Santa Barbara, CA; 690 nm laser) and a variable-wavelength UV detector (Agilent 1100 series), respectively. Data were collected and analyzed by ASTRA software (Wyatt Technology). Displayed data are duplicate 25 μL injection averages of peak areas (voltage signal × volume, V × mL) calculated after baseline correction. Buffer blanks and negative controls (rIAPP) were analyzed intermittently and showed no change in light scattering or UV absorbance over time.

RESULTS

IAPP-Derived Permeabilizing Activity Forms Rapidly and Disappears as Fibrils Appear. Permeabilization of synthetic PG vesicles to calcium was probed by measuring the fluorescence enhancement of the vesicle-encapsulated calcium-sensitive fluorophore Fura-2 (*41*, *42*, *49*). Aliquots were removed from IAPP fibrillization assays run at two temperatures (RT in black and 37 °C in gray, Figure 2B) and analyzed. Incubations containing rIAPP served as negative controls; neither fibrillization nor permeabilizing activity was detected. At the first time point that was analyzed, some

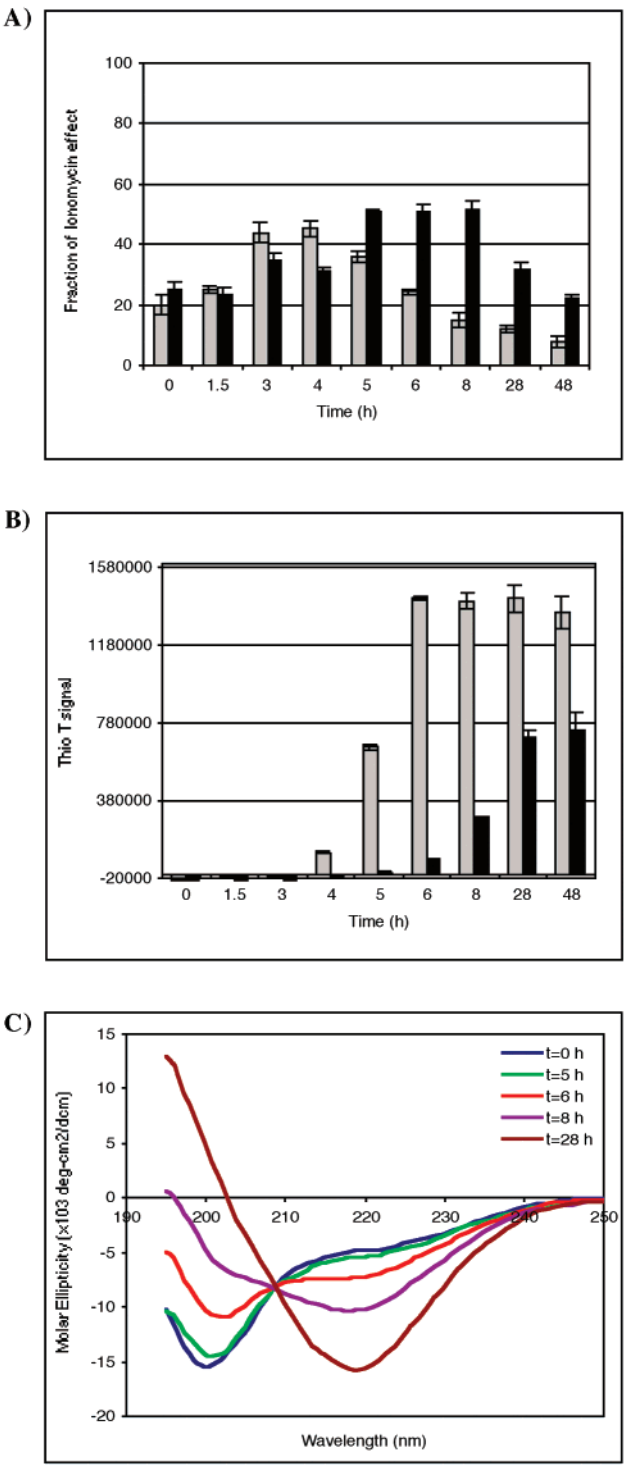

FIGURE 2: Permeabilizing activity forms slowly and then disappears as fibrils grow. (A) The (per mole) effect of IAPP, incubated at 37 °C (gray) or RT (black), on the permeability of egg PG vesicles. Effects are reported as fractions of the ionomycin effect and represent the averages of three or four measurements. Measurements were taken after the peptide-induced calcium flux had come to equilibrium (15 min). (B) Kinetics of IAPP fibril formation in the same incubation, as measured by the thioflavin T method at 37 °C (gray) and RT (black). (C) CD spectra of IAPP measured over time at RT. Measurements were taken in 10 mM Tris buffer, pH 7.0, and 28 μM IAPP.

permeabilizing activity (ca. 20% of the activity of ionomycin in the 37 °C incubation, Figure 2A) was detected, suggesting that either the monomer has activity (rIAPP had none) or some oligomer had formed extremely rapidly, perhaps on

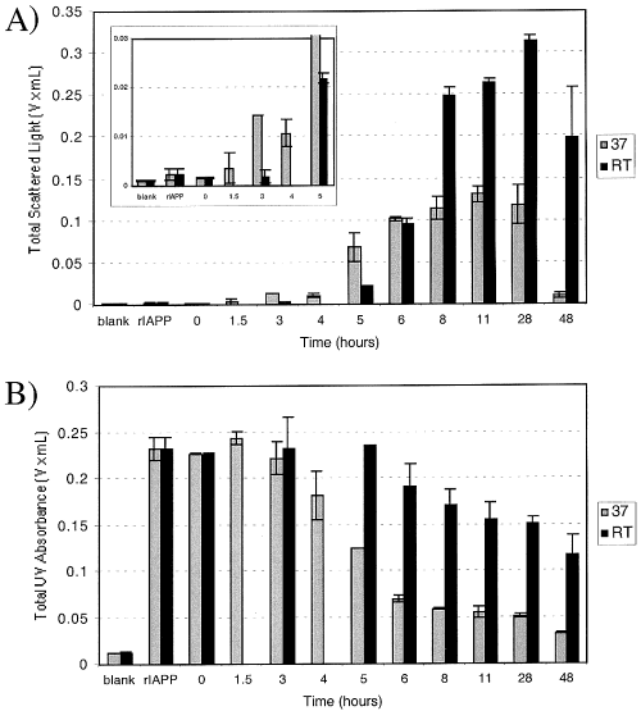

FIGURE 3: Oligomers are detected before insoluble fibrils. (A) Total scattered light of the soluble fractions from RT and 37 °C incubations, plotted as a function of time. (B) Total UV absorbance (220 nm) of the soluble fractions (mixture − fibrils) from RT and 37 °C incubations. The soluble protein concentration remains unchanged for up to 3 h at 37 °C and 5 h at RT (rIAPP was the negative control). Note that an increase in scattered light is a function of both oligomer size and oligomer concentration. For example, the scattered light is approximately the same at 6 h for both RT and 37 °C incubations, whereas the soluble protein concentration is different (Figure 2B). Not all early time points were measured for RT. A significant increase in light scattering is observed by 1.5 and 3 h at 37 °C and by 3 and 5 h at RT. These data correlate well with increases in vesicle permeability at those time points.

the vesicle surface (see below). The activity increased over time in both incubations, reaching a maximum of ca. 45% at 3−4 h in the 37 °C incubation and ca. 50% at 5−8 h in the RT incubation, before declining as fibrils appeared [by 4 h at 37 °C and 6 h at RT, as detected by the thioflavin T assay (Figure 2B) and confirmed by electron microscopy]. The appearance of fibrils was also detected by circular dichroism spectroscopy, which clearly showed the transition from predominantly random coil monomer to β-sheet-rich fibril (minimum at ca. 218 nm, Figure 2C).

Oligomeric IAPP, Comprising a Small Percentage of Total IAPP, Forms Rapidly and Then Is Consumed As Fibrils Appear. Aliquots from the RT (black) and 37 °C (gray) incubations discussed above were centrifuged to remove fibrillar IAPP and then analyzed by UV (220 nm) to measure the amount of total soluble IAPP (monomer plus oligomer) and light scattering (LS) to measure the amount of protofibrillar IAPP (Figure 3). It must be emphasized that the nonfibrillar fraction is heterogeneous, and that the species of interest (see below) are not necessarily the most stable. However, the LS data can be translated to produce an average MW of the nonfibillar (monomer plus protofibrils plus unstructured oligomers) species over time.

At both temperatures (albeit more rapidly at 37 °C), protofibrillar species were detected after 1.5−5 h (Figure 3A), before significant formation of insoluble fibrils (loss of UV absorbance from the soluble phase, Figure 3B). The population of soluble IAPP oligomers grew initially, and then decreased as fibril formation proceeded, consistent with these species being protofibrillar intermediates. The UV absorbance derived from the control incubations containing rIAPP did not change over time (Figure 3B, pair of bars second from left), nor did it scatter light (Figure 3A, inset, second from left).

After incubation for 4 h at 37 °C, when fibrils are just starting to appear and the permeabilizing activity is maximum, the average MW of the nonfibrillar species (fibrils were removed by centrifugation so do not contribute to the LS signal) was 170000−690000 [MW (IAPP) is ca. 4000]. After 28 h at 37 °C, when the Thio T signal had plateaued and the permeabilizing activity had virtually disappeared, the average MW was 675000−1000000. Finally, after 48 h at 37 °C, the average MW of the soluble species decreased to 57000−114000. Also, note that by UV absorbance measurement most of the soluble fraction-containing protofibrils had converted to fibrils by this time.

The Formation of Permeabilizing Activity Was Accelerated by the Presence of Vesicles. The fact that permeabilizing activity was observed (Figure 2A), before oligomers were detected (Figure 3A), contrasted with the case of α-synuclein, where the monomeric protein clearly showed no permeabilizing activity (*41*, *42*). This finding suggested that IAPP may form the permeabilizing species in the presence of vesicles, during the typical 15 min incubation prior to the permeabilization measurement. To test this possibility, aliquots removed at $t = 0$ (all monomer), $t = 6$ h (some protofibril), and $t = 26$ h (fibrils present) were incubated with vesicles for varying times before permeabilization to calcium was assessed (Figure 4A). In each case, the level of permeabilization increased over time, with the 6 h aliquot always showing the greatest effect. This result suggested that monomer, which was present in all three aliquots, oligomerized in the presence of vesicles. Consistent with that proposal, the CD spectrum of IAPP changed over time in the presence of vesicles (Figure 4B), with the level of random coil features decreasing and the level of β-sheet slightly increasing (note the shift in the minimum). At higher IAPP concentrations, an α-helix-to-β-sheet transition was observed (data not shown).

The Permeabilizing IAPP Protofibril, like a Pore, Only Allows Passage of Small Molecules. IAPP produced a much greater degree of permeabilization to calcium than to Fura-2 (MW = 832) and FITC-dextran (MW = 4400) (Figure 5). No significant permeabilization to Fura-2, FITC-dextran, or calcium was induced by rIAPP (data not shown).

DISCUSSION

It is demonstrated here that IAPP protofibrils, like α-synuclein protofibrils, have the ability to permeabilize synthetic vesicles by a pore-like mechanism. The fact that the permeabilization is selective for low-MW molecules rules out the possibility of a "carpet" mechanism (*42*). Several other reports of channel-like activity of IAPP have appeared (*45*−*47*). Unlike the α-synuclein case, where pore-like structures have been detected by AFM (*50*) and EM (*51*, *56*), no such structures have yet been detected in the case of

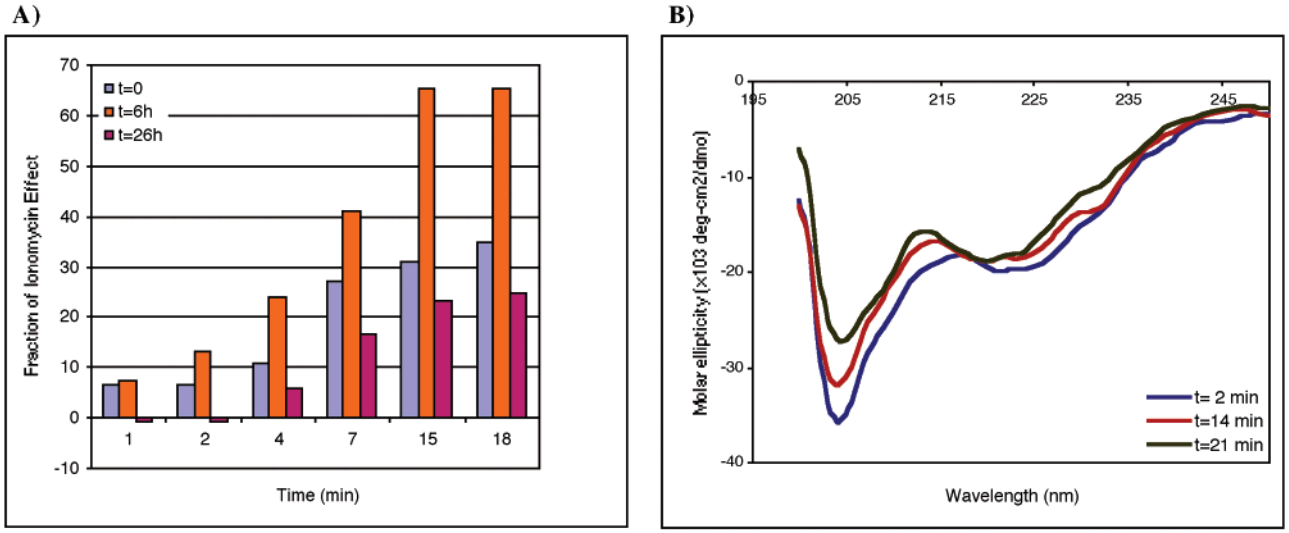

FIGURE 4: Incubation of IAPP with vesicles promotes formation of the permeabilizing species. (A) PG vesicle permeabilization effect induced by IAPP as a function of the duration of incubation with vesicles (experiments in Figure 2 were performed with a 15 min preincubation) and the duration of preincubation of IAPP ($t = 0$ h, $t = 6$ h, and $t = 26$ h). Each data point represents a single measurement. (B) CD spectra of IAPP measured during incubation with vesicles at RT. Note the decrease in negative ellipticity at ca. 205 nm and the slight shift in the position of the higher-wavelength minimum.

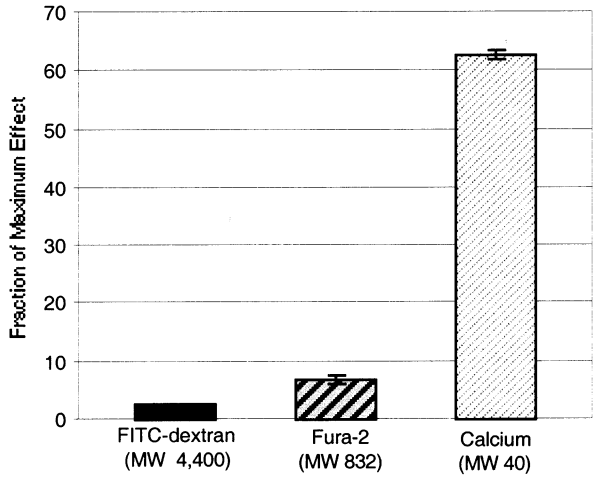

FIGURE 5: The permeabilizing species do not allow large molecules to pass. Measurements were taken as described in the legend of Figure 2. Representative data are expressed as the fraction of the maximum effect and represent the averages of three measurements.

IAPP, most likely for technical reasons. However, the kinetics of IAPP amyloid pore formation and disappearance strongly suggest that the active species is an ordered oligomeric fibrillization intermediate. The active species may be a small oligomer of IAPP, possibly a 20−40mer as may be the case for α-synuclein (*51*, *56*). The LS analysis is hampered by the heterogeneity of the process, but suggests that the active species is larger than a 6mer and that increasing oligomer size beyond a 20−40mer does not necessarily increase the permeabilizing activity.

Although the potential role for IAPP amyloid fibril formation in NIDDM pathogenesis has been discussed (*3*, *4*), the classification of NIDDM as an amyloid disease has not been widely accepted. One potential source of confusion in this regard is the assumption that the fibril itself must be the pathogenic species in an amyloid disease. This incorrect assumption creates criteria that neither NIDDM nor AD and PD fulfill. It is therefore useful to re-examine several controversial features of NIDDM.

First, pancreatic amyloid is not found in all NIDDM patients, but ca. 90% of them. At the same time, a significant fraction of unaffected aged individuals have pancreatic amyloid. Both of these are true of the relationship between brain amyloid and disease/age in AD and PD (*29*) and are expected corollaries of the toxic protofibril model. Second, IAPP-overexpressing transgenic mice do not always develop pancreatic amyloid and/or NIDDM. Again, this is also the case for the transgenic mouse model of PD, where no fibrillar deposits are observed (but extensive nonfibrillar α-synuclein deposits are present) (*52*). Third, IAPP protofibrils have not been directly detected in diseased ex vivo tissue, although fibril-like material has been described in *β*-cell granules in transgenic mice (*53*), in the cytoplasm in cell culture models (*24*, *54*), and in human insulinomas (*55*). The small size and instability of protofibrils make their detection difficult. Finally, the single characterized IAPP missense mutation, S20G (*19*), shows a low frequency (4.1%) in late onset NIDDM (≥50 years), but a relatively high frequency (10%) in early onset disease (≤35 years). It may be that S20G is best thought of as a risk factor. It is important to note that the S20G mutation increases the rate of fibril formation (so does A53T in the α-synuclein case) (*20*, *21*). The effect of this mutation on protofibril formation has not been reported.

Thus, NIDDM shares many essential features with age-associated neurodegenerative diseases that may be triggered by amyloid protofibril formation. We propose that amyloid pores, which seem to be a subpopulation of amyloid protofibrils comprising a variety of disease-associated proteins, may initiate pancreatic *β*-cell death and subsequent pathogenesis.

ACKNOWLEDGMENT

We thank Michael J. Volles and Hilal A. Lashuel for many insightful discussions during the preparation of the manuscript.

REFERENCES

1. Koo, E. H., Lansbury, P. T., Jr., and Kelly, J. W. (1999) *Proc. Natl. Acad. Sci. U.S.A. 96*, 9989−9990.
2. Rochet, J. C., and Lansbury, P. T., Jr. (2000) *Curr. Opin. Struct. Biol. 10*, 60−68.
3. Hoppener, J. W., Ahren, B., and Lips, C. J. (2000) *N. Engl. J. Med. 343*, 411−419.
4. Kahn, S. E., Andrikopoulos, S., and Verchere, C. B. (1999) *Diabetes 48*, 241−253.
5. Clark, A., Cooper, G. J., Lewis, C. E., Morris, J. F., Willis, A. C., Reid, K. B., and Turner, R. C. (1987) *Lancet 2*, 231−234.
6. Ferrannini, E. (1998) *Endocr. Rev. 19*, 477−490.
7. Westermark, P., Engstrom, U., Westermark, G. T., Johnson, K. H., Permerth, J., and Betsholtz, C. (1989) *Diabetes Res. Clin. Pract. 7*, 219−226.
8. Johnson, K. H., O'Brien, T. D., Betsholtz, C., and Westermark, P. (1989) *N. Engl. J. Med. 321*, 513−518.
9. Jaikaran, E. T., and Clark, A. (2001) *Biochim. Biophys. Acta 1537*, 179−203.
10. Castle, A. L., Kuo, C. H., and Ivy, J. L. (1998) *Am. J. Physiol. 274*, E6−E12.
11. Leighton, B., and Cooper, G. J. (1988) *Nature 335*, 632−635.
12. Molina, J. M., Cooper, G. J., Leighton, B., and Olefsky, J. M. (1990) *Diabetes 39*, 260−265.
13. Rink, T. J., Beaumont, K., Koda, J., and Young, A. (1993) *Trends Pharmacol. Sci. 14*, 113−118.
14. Ye, J. M., Lim-Fraser, M., Cooney, G. J., Cooper, G. J., Iglesias, M. A., Watson, D. G., Choong, B., and Kraegen, E. W. (2001) *Am. J. Physiol. 280*, E562−E569.
15. Hettiarachchi, M., Chalkley, S., Furler, S. M., Choong, Y. S., Heller, M., Cooper, G. J., and Kraegen, E. W. (1997) *Am. J. Physiol. 273*, E859−E867.
16. Ashburn, T. T., and Lansbury, P. T., Jr. (1993) *J. Am. Chem. Soc. 115*, 11012−11013.
17. Westermark, P., Engstrom, U., Johnson, K. H., Westermark, G. T., and Betsholtz, C. (1990) *Proc. Natl. Acad. Sci. U.S.A. 87*, 5036−5040.
18. Goldsbury, C., Goldie, K., Pellaud, J., Seelig, J., Frey, P., Muller, S. A., Kistler, J., Cooper, G. J., and Aebi, U. (2000) *J. Struct. Biol. 130*, 352−362.
19. Sakagashira, S., Sanke, T., Hanabusa, T., Shimomura, H., Ohagi, S., Kumagaye, K. Y., Nakajima, K., and Nanjo, K. (1996) *Diabetes 45*, 1279−1281.
20. Westermark, G. T., and Westermark, P. (2000) *Amyloid 7*, 19−22.
21. Sakagashira, S., Hiddinga, H. J., Tateishi, K., Sanke, T., Hanabusa, T., Nanjo, K., and Eberhardt, N. L. (2000) *Am. J. Pathol. 157*, 2101−2109.
22. Lorenzo, A., Razzaboni, B., Weir, G. C., and Yankner, B. A. (1994) *Nature 368*, 756−760.
23. O'Brien, T. D., Butler, P. C., Kreutter, D. K., Kane, L. A., and Eberhardt, N. L. (1995) *Am. J. Pathol. 147*, 609−616.
24. Hiddinga, H. J., and Eberhardt, N. L. (1999) *Am. J. Pathol. 154*, 1077−1088.
25. Janson, J., Soeller, W. C., Roche, P. C., Nelson, R. T., Torchia, A. J., Kreutter, D. K., and Butler, P. C. (1996) *Proc. Natl. Acad. Sci. U.S.A. 93*, 7283−7288.
26. Verchere, C. B., D'Alessio, D. A., Palmiter, R. D., Weir, G. C., Bonner-Weir, S., Baskin, D. G., and Kahn, S. E. (1996) *Proc. Natl. Acad. Sci. U.S.A. 93*, 3492−3496.
27. MacArthur, D. L., de Koning, E. J., Verbeek, J. S., Morris, J. F., and Clark, A. (1999) *Diabetologia 42*, 1219−1227.
28. Hoppener, J. W., Oosterwijk, C., Nieuwenhuis, M. G., Posthuma, G., Thijssen, J. H., Vroom, T. M., Ahren, B., and Lips, C. J. (1999) *Diabetologia 42*, 427−434.
29. Lansbury, P. T., Jr. (1999) *Proc. Natl. Acad. Sci. U.S.A. 96*, 3342−3344.
30. Goldberg, M. S., and Lansbury, P. T., Jr. (2000) *Nat. Cell Biol. 2*, E115−E119.
31. Harper, J. D., and Lansbury, P. T., Jr. (1997) *Annu. Rev. Biochem. 66*, 385−407.
32. Conway, K. A., Lee, S. J., Rochet, J. C., Ding, T. T., Williamson, R. E., and Lansbury, P. T., Jr. (2000) *Proc. Natl. Acad. Sci. U.S.A. 97*, 571−576.
33. Walsh, D. M., Lomakin, A., Benedek, G. B., Condron, M. M., and Teplow, D. B. (1997) *J. Biol. Chem. 272*, 22364−22372.
34. Harper, J. D., Lieber, C. M., and Lansbury, P. T., Jr. (1997) *Chem. Biol. 4*, 951−959.
35. Conway, K. A., Harper, J. D., and Lansbury, P. T., Jr. (1998) *Nat. Med. 4*, 1318−1320.
36. Lashuel, H. A., Zhihong, L., and Kelly, J. W. (1998) *Biochemistry 37*, 17851−17864.
37. Goldsbury, C., Kistler, J., Aebi, U., Arvinte, T., and Cooper, G. J. (1999) *J. Mol. Biol. 285*, 33−39.
38. Padrick, S. B., and Miranker, A. D. (2001) *J. Mol. Biol. 308*, 783−794.
39. Padrick, S. B., and Miranker, A. D. (2002) *Biochemistry 41*, 4694−4703.
40. Hartley, D. M., Walsh, D. M., Ye, C. P., Diehl, T., Vasquez, S., Vassilev, P. M., Teplow, D. B., and Selkoe, D. J. (1999) *J. Neurosci. 19*, 8876−8884.
41. Volles, M. J., Lee, S. J., Rochet, J. C., Shtilerman, M. D., Ding, T. T., Kessler, J. C., and Lansbury, P. T., Jr. (2001) *Biochemistry 40*, 7812−7819.
42. Volles, M. J., and Lansbury, P. T., Jr. (2002) *Biochemistry 41*, 4595−4602.
43. Jaikaran, E. T., Higham, C. E., Serpell, L. C., Zurdo, J., Gross, M., Clark, A., and Fraser, P. E. (2001) *J. Mol. Biol. 308*, 515−525.
44. Janson, J., Ashley, R. H., Harrison, D., McIntyre, S., and Butler, P. C. (1999) *Diabetes 48*, 491−498.
45. Mirzabekov, T. A., Lin, M. C., and Kagan, B. L. (1996) *J. Biol. Chem. 271*, 1988−1992.
46. Kawahara, M., Kuroda, Y., Arispe, N., and Rojas, E. (2000) *J. Biol. Chem. 275*, 14077−14083.
47. Harroun, T. A., Bradshaw, J. P., and Ashley, R. H. (2001) *FEBS Lett. 507*, 200−204.
48. Hirakura, Y., Yiu, W. W., Yamamoto, A., and Kagan, B. L. (2000) *Amyloid 7*, 194−199.
49. Blau, L., and Weissmann, G. (1988) *Biochemistry 27*, 5661−5666.
50. Ding, T. T., Lee, S. J., Rochet, J. C., and Lansbury, P. T., Jr. (2002) *Biochemistry 41*, 10209−10217.
51. Lashuel, H. A., Petre, B., Wall, J. S., Simon, M., Nowak, R., Walz, T., and Lansbury, P. T., Jr. (2002) *J. Mol. Biol.* (in press).
52. Masliah, E., Rockenstein, E., Veinbergs, I., Mallory, M., Hashimoto, M., Takeda, A., Sagara, Y., Sisk, A., and Mucke, L. (2000) *Science 287*, 1265−1269.
53. Yagui, K., Yamaguchi, T., Kanatsuka, A., Shimada, F., Huang, C. I., Tokuyama, Y., Ohsawa, H., Yamamura, K., Miyazaki, J., Mikata, A., et al. (1995) *Eur. J. Endocrinol. 132*, 487−496.
54. de Koning, E. J., Morris, E. R., Hofhuis, F. M., Posthuma, G., Hoppener, J. W., Morris, J. F., Capel, P. J., Clark, A., and Verbeek, J. S. (1994) *Proc. Natl. Acad. Sci. U.S.A. 91*, 8467−8471.
55. O'Brien, T. D., Butler, A. E., Roche, P. C., Johnson, K. H., and Butler, P. C. (1994) *Diabetes 43*, 329−336.
56. Lashuel, H. A., Hartley, D., Petre, B. M., Walz, T., and Lansbury, P. T., Jr. (2002) *Nature 418*, 291.

BI020314U